Can laminated carbon challenge gold? Towards universal, scalable and low-cost carbon electrodes for perovskite solar cells

Gaveshana A. Sepalage, Hasitha Weerasinghe, Nitish Rai, Noel Duffy, Sonia R. Raga, Yvonne Hora, Mei Gao, Doojin Vak, Anthony S. R. Chesman, Udo Bach, Alexandr N. Simonov

Dr G. A. Sepalage, Dr A. N. Simonov
School of Chemistry, Monash University, 3800 Victoria, Australia
E-mail: alexandr.simonov@monash.edu

Dr G. A. Sepalage, N. Rai, Dr S. R. Raga, Y. Hora, Prof U. Bach
Department of Chemical Engineering, Monash University, 3800 Victoria, Australia
E-mail: udo.bach@monash.edu

Dr H. Weerasinghe, Dr M. Gao, Dr D. Vak, Dr A. S. R. Chesman
CSIRO Manufacturing, Research Way, CSIRO, Clayton, 3169 Victoria, Australia
E-mail: hasitha.weerasinghe@csiro.au

Dr N. Duffy
CSIRO Energy, Clayton, 3169 Victoria, Australia

Dr S. R. Raga
Institut Català de Nanociència i Nanotecnologia, Universitat Autònoma de Barcelona, 08193 Bellaterra, Barcelona, Spain

Prof U. Bach
ARC Centre of Excellence in Exciton Science, Monash University, 3800 Victoria, Australia

Dr A. N. Simonov
ARC Centre of Excellence for Electromaterials Science, Monash University, 3800 Victoria, Australia

Abstract

While perovskite solar cell (PSC) efficiencies are soaring at a laboratory scale, these are most commonly achieved with evaporated gold electrodes, which would present a significant expense in large-scale production. This can be remedied through the use of significantly cheaper carbon electrodes that also do not migrate through the device in contrast to metals. To this end, the present work investigates simple to prepare aluminium-supported carbon electrodes derived from inexpensive materials directly available from commercial suppliers that can be applied onto various hole-transporting materials and enable photovoltaic performances on par with that provided by gold electrodes. Successful integration of the new carbon-based electrode into flexible devices produced by a roll-to-roll printing technology by both pressing and lamination is demonstrated. However, temperature cycling durability tests reveal that the use of carbon electrodes based on commercial pastes is hindered by incompatibility of adhesive additives with the key components of the PSCs under heating. Resolving this issue, we introduce tailor-made graphite electrodes devoid of damaging additives, which improve the PSC stability under temperature cycling test protocol to the level provided by benchmark gold electrodes. The study highlights current challenges in developing laminated carbon electrodes in PSCs and proposes strategies towards the resolution thereof.

1. Introduction

Studies on perovskite solar cells (PSC) have overwhelmingly focussed on increasing device performance, which has resulted in an unprecedented pace of improvement in the technology. However, these investigations often use materials which are expensive or not earth abundant, and therefore do not take into consideration the cost of the devices if they were to be produced at scale.[1] While electron-transporting materials (ETM) and perovskite photoabsorbers, as well as the methods for their deposition, are indeed cheap and scalable, this does not extend to other key components of the cells, *viz*. some of the most popular hole-transporting materials (HTM), as well as the transparent and counter electrodes commonly used in contemporary research.[2],[3] Of particular concern is the near ubiquitous use of thin layers of gold as the counter electrode, which seem to be an irreplaceable component of all major record-breaking perovskite solar cells.[4–8] A simple calculation based on a typical Au layer thickness (*ca* 80 nm) and the current price of this metal, which is highly volatile,[9] indicates a cost of approximately 100 USD per square meter for only the PSC top electrode. This can be compared to the current total cost of manufacturing state-of-the-art silicon photovoltaics of only *ca* 50 USD m^{-2}.[10] The cost and technical challenges associated with upscaling of high-vacuum thermal evaporation techniques raise additional concerns in respect to their broad industrial application.[11] Furthermore, evidence exists of the migration of gold to the perovskite through the HTM, resulting in an irreversible deterioration of the performance.[12]

Taken together, these factors question the feasibility of using gold electrodes in commercial PSCs. Indeed, the reported cost-efficiency studies of perovskite photovoltaics never recommend the use of Au, but consider much cheaper electrode materials, such as copper and silver.[2] However, direct replacement of gold with other metals is often challenging in a standard *n-i-p* configuration, as those suffer rapid corrosion in operation and thereby induce fast degradation of the whole device, especially when exposed to ambient environment and moisture.[13–16]

An appealing alternative to metal-based electrodes in PSCs is carbon – an inexpensive material that has been widely used as a conductor in a variety of scientific and industrial processes and equipment,[17–19] including in perovskite photovoltaics.[20–22] In addition to its low cost and abundance, the useful properties of carbon include a suitable work function (-5.0 eV[23]; *cf.* to -5.1 eV for Au[24]), high electrochemical stability[22] and tuneable hydrophobicity,[25,26] which can endow devices with an additional protection mechanism against penetration of H_2O – a well-known foe for the perovskite light-harvesters.[27] Furthermore, specific carbon-based materials can be designed to function as hole-selective charge extraction layers, though their performance still requires improvements and the best results are often achieved in combination with conventional HTMs.[28–31] At this point, it is also important to differentiate between different carbon allotropes: while graphite and carbon black can be indeed considered relatively cheap and available, more specialised materials like single-walled carbon nanotubes cannot. Indeed, the price for high-quality nanotubes made *via* chemical vapour deposition, as required for application in high efficient PSCs,[32–34] is currently comparable to that of gold.[9] Therefore, whenever carbon is discussed as a promising electrode material below, truly cheap allotropes such as graphite and carbon black are considered only.

To prepare a conventional *n-i-p* perovskite solar cell, a carbon electrode can be deposited using one of several simple and scalable techniques: doctor blading and screen printing, press transfer from another substrate and direct lamination. Direct doctor blading and screen printing are considered the easiest, fastest and most broadly applied approaches,[35,36] but the solvents and additives contained in the deposited carbon paste may unfavourably alter the underlying layers, resulting in deterioration of the device performance. Overcoming these issues, a screen printed carbon layer can be first formed, annealed at high temperature to remove all undesired compounds and then infiltrated with perovskite, as reported by Han and co-workers.[23,37] This innovative and highly insightful approach resulted in notably improved operational stability, though the demonstration of devices with high PCE based on this architecture is yet to be

reported. Possibly, this might be achieved through further improvements in the pore filling, suppressing the defect density in the perovskite absorber and enhancements in the charge extraction at the perovskite|HTM interface. Alternatively, other strategies to introduce carbon electrodes into PSCs can be considered.[38] Particularly attractive are press transfer and lamination, where a dried carbon film devoid of solvents immobilised on a suitable substrate is pressed onto the device.[39,40] In the first case, the substrate is removed and can be reused, while the laminated electrode-substrate assembly is not separated and its deposition completes the device fabrication. Some of the key results achieved by press transfer and lamination of carbon electrodes onto PSCs are briefly surveyed below.

Several studies focused on pressing of a carbon layer onto the perovskite followed by infiltration of a HTM, although introduction of expensive, high-quality single-walled carbon nanotubes was required to achieve reasonable efficiencies ranging from *ca* 10%[41] to 16.8 ± 0.5%.[42] Other work, more relevant to the present study, avoided the HTM-infiltration approach, as well as the expensive nanotube component. For example, the hot-pressing of a carbon film onto a FTO|TiO_2|$CH_3NH_3PbI_3$ (FTO = fluorine-doped tin(IV) oxide) assembly was reported to produce HTM-free solar cells with an average efficiency of *ca* 12% in 2015.[38] A similar approach was employed to hot press a carbon film onto FTO|SnO_2|$CsFA_{0.83}MA_{0.17}PbI_{2.53}Br_{0.47}$|CuSCN, resulting in a PCE of 14.6 ± 0.4%.[43] An important achievement in the field was made in 2018 through the demonstration of a power conversion efficiency of *ca* 19% for a perovskite solar cell with a carbon film electrode (*cf.* 20 % for a Au-based control) derived from a commercial adhesive paste and pressed on top of a HTM layer.[39] Importantly, these devices also demonstrated reasonable short-term (80 h) stability under continuous illumination at 20 °C in N_2. Unfortunately, achieving scalable and reproducible results has proven difficult with this approach, in particular, due to the lack of a robust substrate to hold the carbon electrode during the pressing process and limited control over pressing conditions. To address this, the same team reported an upgraded methodology in

2019 based on a carbon cloth and aluminium foil as substrates for the carbon electrode, but achieved lower PCEs of 15 ± 2 % and 12 ± 2 %, respectively (*cf.* 18 ± 1 % for the Au-based control).[40] The preliminary stability data reported in this work demonstrated the advantage of using carbon on a carbon cloth compared to gold, while the aluminium substrate was found to partially exfoliate from the electrode, resulting in deteriorated initial efficiency and stability and overall decreased reproducibility of the results.

Thus, the applicability of carbon electrodes for high-performance PSCs has been demonstrated at the research level. A desirable further development in the carbon electrodes for PSCs would be the establishment of a procedure that can be integrated into a roll-to-roll solar cell fabrication process. Such technologies are being developed by a range of teams, for example by CSIRO who demonstrated a roll-to-roll slot-die coating procedures for perovskite, electron selective and hole selective materials enabling the high-throughput production of flexible PSCs with an efficiency of up to 11%.[44] The downside of this promising result is the reliance on the evaporated metal electrodes, which replacement with laminatable carbon would significantly advance the technology. We note again that it is important to develop such carbon electrodes using cheap materials like graphite flakes and carbon black, which are produced in large quantities and of comparable quality worldwide, to enable reproducibly high performance and promote commercialisation.

The present work aims to support these developments and expand the usability of the carbon-based electrodes in PSCs through the demonstration of a universal “sticker-like” electrode that (i) can be applied onto chemically different surfaces like organic and inorganic HTMs, (ii) provides a solar cell performance not worse than the benchmark evaporated gold, and (iii) is suitable for integration into a roll-to-roll solar cell fabrication process. Fabrication and deposition of the final configuration of the electrodes presented herein is based on relatively cheap commercial components (total cost of *ca* 2 USD m^{-2}) and only basic laboratory equipment. At the same time, we also highlight the new stability challenges arising from the use of the

adhesive-modified commercial carbon pastes and outline the pathway for the future developments.

2. Results and discussion

2.1. Electrode fabrication

The overall procedure for the fabrication and application of the carbon-based electrodes introduced herein onto a perovskite solar cell (PSC) is technically simple and scale flexible (**Figure 1**). The electrode consists of two major components – a carbon layer that can attach to different HTM surfaces and a highly conductive, flexible and mechanically stable substrate. The important role of the latter will be discussed further in the text. Among a range of possible substrate options, we have selected a low cost, readily available and easy to handle material – a conventional general-purpose aluminium foil with a thickness of *ca* 12 μm.

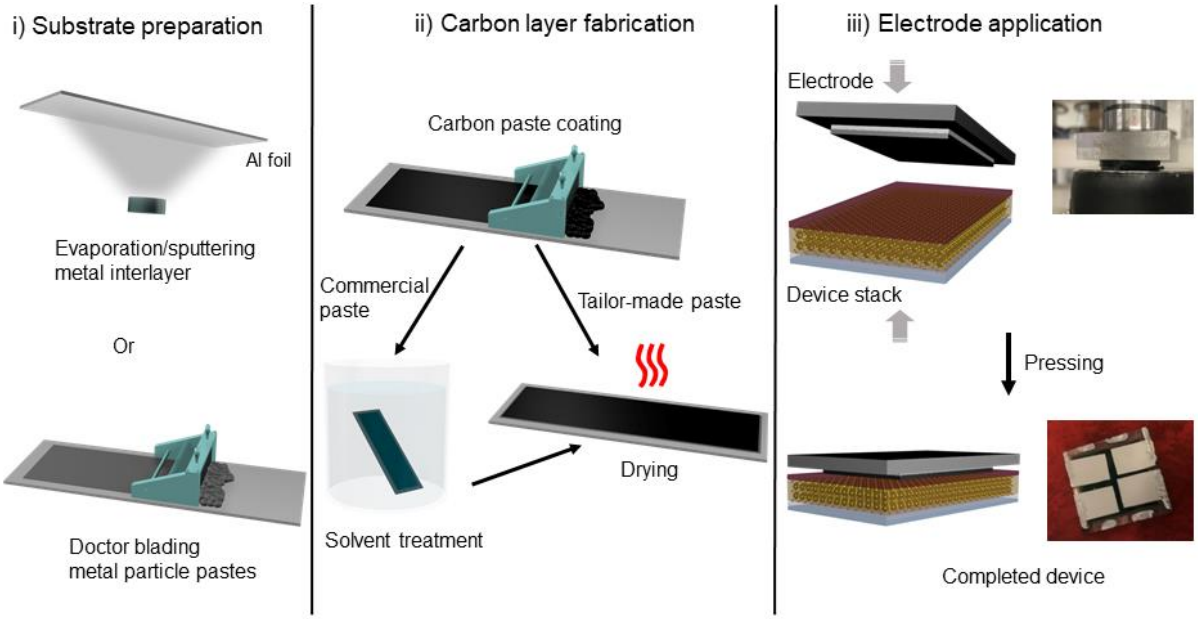

Figure 1. Schematic summary of the fabrication of perovskite solar cells with a laminatable carbon|aluminium electrode: (I) preparation of an aluminium substrate through the deposition of a metal interlayer; (II) deposition of the carbon layer onto the aluminium substrate; (III) application of the carbon|aluminium electrodes onto the solar cell.

In step I, the aluminium substrate surface is modified with a thin metal interlayer, which can be produced either by sputtering or evaporation techniques, or most conveniently, by doctor

blading a metal nanoparticle paste. There are no strict requirements for the thickness of this interlayer, and it was arbitrarily set to approximately 80 nm for evaporated/sputtered metals and approximately 25 µm thick for the doctor bladed coating. This interlayer substantially improves electrical connection between carbon and aluminium, as will be discussed in detail later in the paper. Step II is casting of the carbon layer by doctor-blading of a commercial or tailor-made paste. An important additional step that should be applied if the commercial carbon paste is used is washing with ethanol to remove residual organic compounds that are not easily evaporated and are detrimental to the device components.[39] The device parameters show no significant variations in the performance over a range of carbon electrode thickness from 20 to 100 µm (**Figure S1**). Complete carbon|aluminium electrodes are then dried in air to remove solvents. In step III, the electrode cut to the required size is applied onto a device by simple mechanical pressing. Device performance was independent of the applied pressure in the range from 10 to 24 MPa, with a slightly reduced performance at around 8 MPa (**Figure S2**); all data presented below were obtained with an electrode application pressure of 20 MPa. The supplementary video demonstrates the key fabrication procedures summarised in Figure 1. In what follows, the characteristics of the perovskite solar cells based on the carbon|aluminium electrode, as well as the importance of the electrode substrate and metal interlayer, are discussed.

2.2. Glass-supported devices: carbon *vs.* gold electrode

Non-flexible solar cells investigated herein were supported on a transparent glass substrate coated with FTO, which was further modified sequentially with compact (c-TiO_2) and mesoporous titania layers (m-TiO_2), multi-cation and dual-anion $K_{0.05}Cs_{0.25}FA_{1.30}MA_{0.23}Pb_{1.4}I_{2.7}Br_{0.46}$ perovskite, a hole-transporting material, and finally, an electrode. As a HTM, either spiro-OMeTAD, CuSCN or PTAA were used, while the electrodes were either carbon|interlayer|aluminium or evaporated gold.

Analysis of the carbon electrode layer by cross-sectional scanning electron microscopy revealed the expected morphology of coalesced micron-sized aggregates and graphite sheets (**Figure 2**a). Higher magnification images taken at the boundary between the carbon and the spiro-OMeTAD HTM layers indicate a continuous and efficient connection between the two (Figure 2b). The HTM and perovskite layers are not damaged by the pressing process as also seen in SEM micrographs (Figure 2b), which likely indicates uniform pressure distribution during pressing due to the flexibility of the electrode. Imaging of the C|interlayer|Al interface was complicated by the flexible nature of the aluminium substrate. Hence, analysis of the devices that were cracked after peeling off the foil was undertaken to reveal that the thin metal interlayer deposited in fabrication step I (Figure 1) remained firmly attached to the carbon layer (Figure 2c). This is the first indication of the importance of this interlayer, which was further confirmed by the photovoltaic characterisation of the devices.

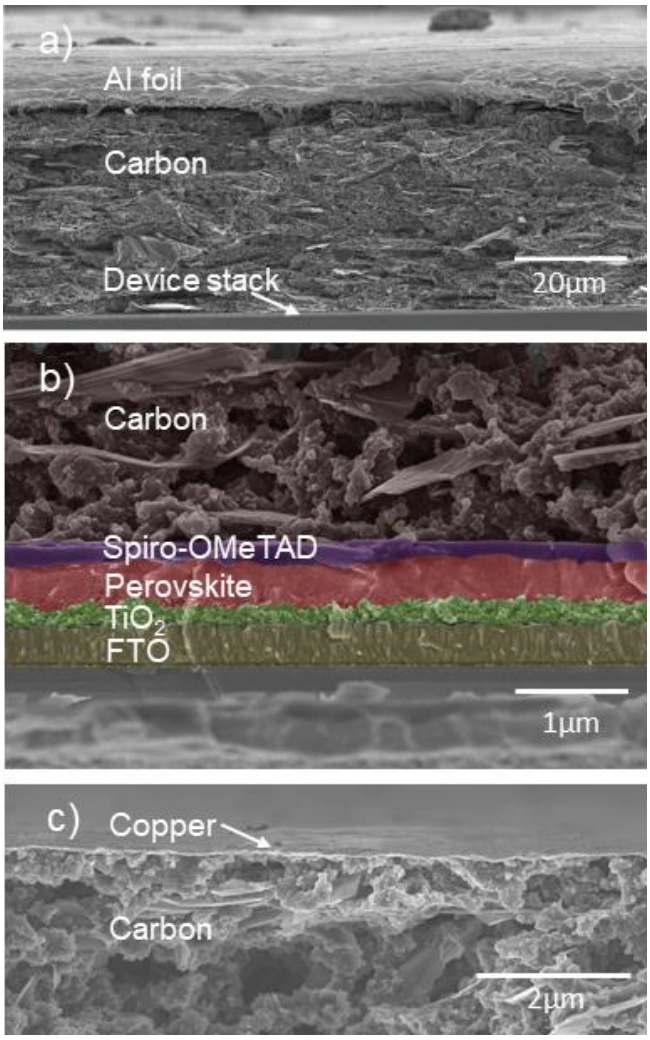

Figure 2. Cross-sectional scanning electron micrographs of the FTO|c-TiO_2|m-TiO_2|$K_{0.05}Cs_{0.25}FA_{1.30}MA_{0.23}Pb_{1.4}I_{2.7}Br_{0.46}$|spiro-OMeTAD|C|Al device with a copper interlayer in the electrode focusing on (a) a carbon electrode layer, (b) carbon|HTM interface, and (c) interface between carbon and Cu interlayer (Al foil was peeled off in this case).

Preliminary assessment of the performance of the PSCs with different modifications of the carbon-based electrode through recording *J-V* curves revealed the critical role of the substrate and the additional layer between C and Al. Indeed, the efficiency of solar cells with a carbon layer only (no interlayer was introduced and Al foil was peeled-off prior to the analysis; contact was provided by soldering to the C layer) was strongly suppressed by a significant series resistance, resulting in extremely low fill factor values (**Figure 3**a, **Tables S1** and **S2**). Keeping the aluminium foil on top of the carbon layer alleviated the series resistance problem and improved the fill factor significantly (Figure 3a and Table S2). Similar findings were previously reported by Su *et al.*[40] and likely indicate insufficient lateral conductivity of the carbon layer

derived from the commercial paste. However, even with the Al substrate present, the photocurrent density was still lower than the photocurrent density observed for the gold electrode (Figure 3a and Table S2). This loss of performance might be associated with the imperfect adhesion of carbon to the smooth foil surface inherently covered by a thin oxide layer. To confirm this hypothesis, an additional interlayer of either gold, copper or nickel was deposited onto Al before depositing carbon (step I in Figure 1). Such simple modification increased the photocurrent by approximately 2.5 mA cm^{-2}, and most important was the independence of this improvement of the chemical nature of the interlayer metal (Figure 3b and Table S2). Thus, the use of only low-cost metals and carbon decreases the overall material cost of the electrode to less than *ca* 2 USD m^{-2} (**Table S3**).

To avoid the use of evaporation/sputtering techniques in the fabrication of the electrode, we further sought a method to introduce a metal interlayer in a manner that is more instrumentally accessible and easier to scale up. It turned out that simple doctor blading of a paste of silver metal particles followed by mild annealing is sufficient for this purpose (second option of step I in Figure 1). The effectiveness of this approach is demonstrated herein with a commercial silver paste diluted with 2-butoxyethanol to attain a rheology suitable for doctor blading. Cross-sectional SEM characterisation again confirms uniform contact between the aluminium substrate, silver interlayer and carbon (**Figure S3**). The performance of the devices with such an interlayer was similar to that achieved with other carbon-based electrodes examined in this study (Figure 3b and Table S2). Hence, the evaporated metal interlayer in the carbon-aluminium assembly can be replaced with a doctor-bladed metal nanoparticulate layer, which is technologically simpler, much easier to scale up, and can be further optimised to improve the performance.

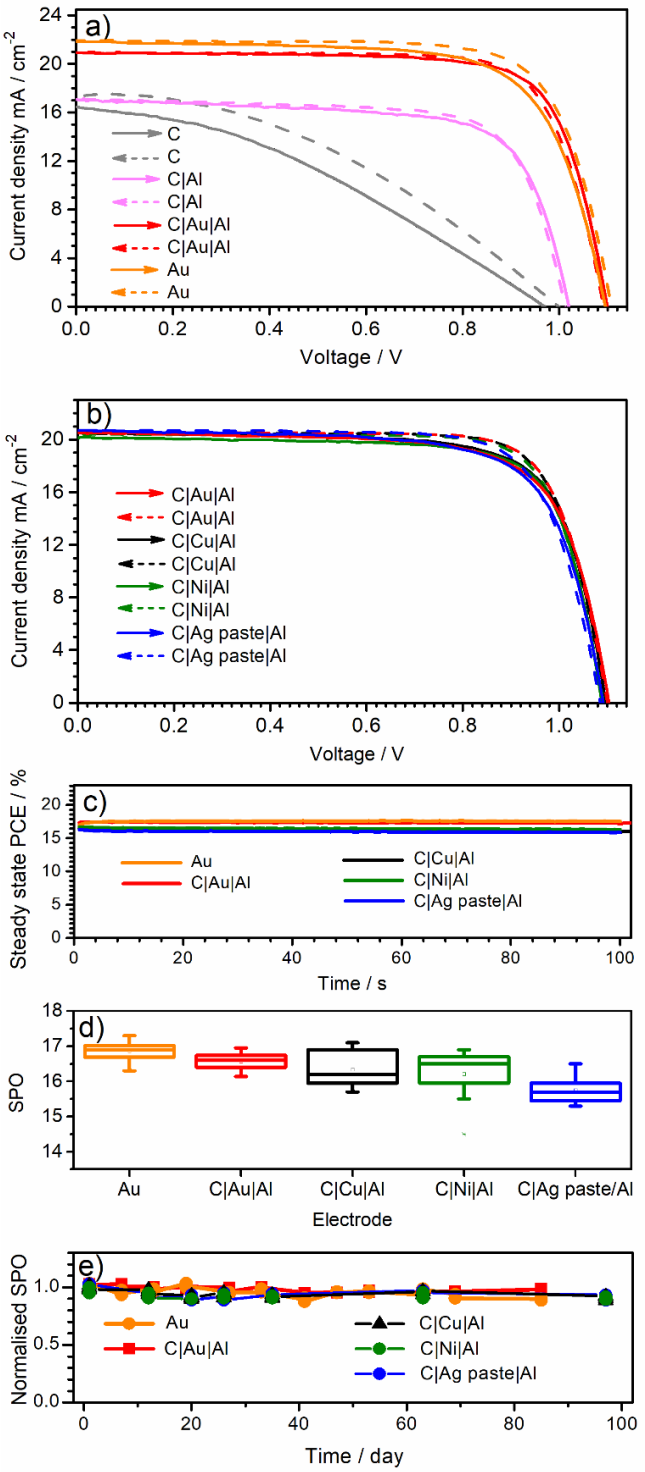

Figure 3. (a-b) Photocurrent-voltage characteristics (0.100 V s^{-1}; scanning directions shown by arrows; 1 sun) and stability of the FTO|c-TiO_2|m-TiO_2|$K_{0.05}Cs_{0.25}FA_{1.30}MA_{0.23}Pb_{1.4}I_{2.7}Br_{0.46}$|spiro-OMeTAD|electrode devices based on different electrodes: (a) carbon only (*grey*), C|Al with no interlayer (*magenta*), C|Au|Al (*red*), Au (*orange*); (b) C|Au|Al (*red*), C|Cu|Al (*black*), C|Ni|Al (*green*), and C|Ag paste|Al (*blue*). (c) Steady state performance at 0.88 (Au, C|Cu|Al, C|Ag paste|Al) and 0.90 V (C|Au|Al, C|Ni|Al). (d) Distribution of the steady-state power output (SPO) for the devices based on Au (n = 20), C|Au|Al (n = 20), C|Cu|Al (n = 8), C|Ni|Al (n = 8) and C|Ag-paste|Al (n = 8) electrodes. Stability of non-encapsulated devices during storage at room temperature and average 10 % relative humidity in the dark.

It is well known that the PSC efficiencies are strongly dependent on a variety of parameters, including the source of materials, laboratory and glove-box environment, device architecture and size, and other subtler factors. Therefore, in order to compare the performance of the carbon-based PSC with a conventional architecture comprising an evaporated gold electrode, we fabricated PSCs with such and carbon-based electrodes which were otherwise identical. Under non-stationary conditions of *J–V* scans, the only slight difference in the parameters of the PSCs based on Au and C|metal|Al electrodes was in the short-circuit current density, which might be theoretically attributed to the lack of the back reflection from the carbon layer, compared to the evaporated Au layer (Figure 3a and Table S2). More important is that the actual performance, *viz.* the stabilised power output measured at the potential of maximal power output derived from the *J-V* data, was essentially identical throughout 20 devices based on Au (16.9 ± 0.3 %) and C|Au|Al (16.6 ± 0.2 %) electrodes. Very similar was the average performance for 8 devices based on C|Cu|Al (16.3 ± 0.5 %), C|Ni|Al (16.5 ± 0.1%) and C|Ag paste|Al (15.8 ± 0.4%) (Figure 3d and Table S2). We also note that the stabilised PCE recorded here for C|interlayer|Al electrodes was higher and more reproducible than reported previously for another version of the aluminium-supported carbon electrode without a metal interlayer (15 ± 2%).[40]

The effect of the electrode on the storage stability was investigated under low relative humidity over twelve weeks (Figure 3e). The observed negligible changes in the performance were essentially identical for Au, C|Au|Al, C|Cu|Al, C|Ni|Al and Cu|Ag-paste|Al, indicating that the use of the carbon-based electrodes with different interlayers does not induce any undesired degradation processes or delamination during storage. This again contrasts the previous report on the interlayer-free aluminium-supported carbon electrodes, which lost more than 35% of the initial device performance over 9 weeks.[40] This loss was insightfully interpreted by the authors by the unsatisfactory mechanical connection between carbon and aluminium – a problem that has been resolved herein through the introduction of the metal interlayer.

To reinforce the conclusions on the effectiveness of the carbon-based electrodes for their use in PSCs derived from the photovoltaic performance results, we have additionally quantified and compared the contact ($R_{contact}$) and recombination (R_{rec}) resistance in the devices based on Au and C|Cu|Al by impedance spectroscopy. The analysed devices were identical except for the electrode, so any differences detected could be confidently ascribed to the HTM|electrode interface. Impedance spectra recorded with the two types of electrodes were very similar, displaying the characteristic two arcs at high and low frequencies. The equivalent circuit introduced by Bisquert *et al.*[45] (**Figure 4**a) was employed to fit the data. Constant phase elements (*CPE*) were used to account for non-ideality of the capacitive elements present.[46] $R_{contact}$ is the resistance originating from external wiring, FTO, metal contacts and the conducting carbon electrode. R_{rec} is the average bulk and interfacial recombination resistance of the perovskite in parallel with the geometric capacitance (CPE_g) of the device. The low-frequency response of the impedance is known to be influenced by the slow-moving ions within the perovskite.[46] This low frequency feature is modelled in the circuit as a parallel "ionic" branch with analogies to a dielectric relaxation (dr), with a resistor (R_{dr}) and CPE_{dr} in series.[45] The physical meaning of these low-frequency parameters is still under debate, as in particular discussed by Yoo *et al.*[46] However, it is generally agreed that R_{dr} originates in the perovskite layer of the device or at its interfaces, and therefore any differences observed in our data would be caused by changes in the perovskite film induced by the application of the carbon *vs.* gold electrode.

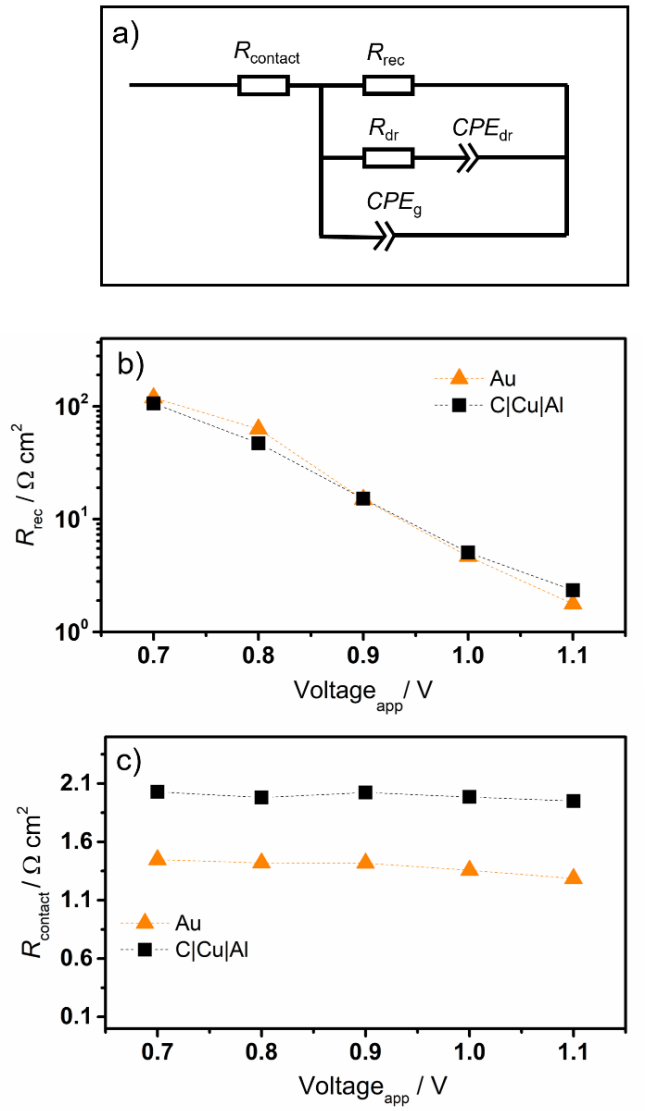

Figure 4. Impedance spectroscopic analysis of the FTO|c-TiO_2|m-TiO_2|$K_{0.05}Cs_{0.25}FA_{1.30}MA_{0.23}Pb_{1.4}I_{2.7}Br_{0.46}$|spiro-OMeTAD|electrode devices based on Au (*orange*) and C|Cu|Al (*black*) electrodes: (a) equivalent circuit used for the data fitting, (b) recombination resistance and (c) contact resistance. Lines in panels (b-c) are guides to the eye. Other fitting parameters are provided in **Table S4**.

The R_{rec} measured with carbon-based and gold electrodes demonstrated minimal differences (Figure 4b), in agreement with the almost identical *J-V* curve performances of the devices (Figure 3a and Figure S4). Moreover, similar values of R_{dr} (Table S4), which reflect the ionic transport/accumulation in the perovskite bulk and interfaces, suggests that the compressive impact applied during the deposition of the C|Cu|Al electrode is not inducing structural damage in the perovskite film or its interfaces with the neighbouring layers. In addition, the $R_{contact}$ for the carbon-based electrode was only 0.5 Ω cm^2 higher than that for Au (Figure 4c), revealing

that the conductivity of the carbon-based electrode is sufficiently high and that high quality ohmic contacts at the C|HTM and C|Cu|Al interface were created. Such a small additional series resistance does not introduce substantial ohmic voltage losses at a current density of the order of 20 mA cm^{-2}, and therefore minimally affects the fill factor.

2.3. Lamination of the carbon-based electrode onto flexible solar cells and different HTMs

Further, we aimed to investigate if the carbon-based electrodes can be applied to other surfaces and in other cell configurations. While being one of the most popular and best-performing HTMs, spiro-OMeTAD also presents some limitations,[47–49] which motivates the development and use of alternative hole-transporters. Therefore, we wanted to test if the carbon-based electrodes described in the present study would be compatible with some of these alternatives in particular with inorganic CuSCN and polymeric PTAA, both being routinely used in PSC research.[4,50,51] Similar to the case of the spiro-OMeTAD benchmark solar cells discussed above, the *J-V* performance of the devices based on two other examined HTMs did not show any significant effects of replacing the evaporated gold with aluminium-supported carbon electrode, even without additional optimisation of the deposition procedures (**Figure S5** and Table S2). Therefore, we conclude that the carbon electrode is compatible not only with the small-molecule spiro-OMeTAD HTM surface, but also with inorganic and polymeric materials. Next, we aimed to investigate the compatibility of the carbon electrode with flexible PSC devices. To this end, tests of pressing the aluminium-supported carbon electrode onto the roll-to-roll printed solar cells fabricated at CSIRO were conducted (**Figure 5**a). Using the same procedures for the electrode fabrication and pressing as those described above (Figure 1), firm attachment of the carbon layer to the cell was achieved (Figure 5b; note that cutting the cell with a paper blade distorted the constituent layers of the solar cell, which prevented quality imaging thereof). The steady-state power conversion efficiency of the device prepared in this manner was 10.0 ± 0.8 % (Figure 5c), which is a promising result since it is very close to the

recently reported roll-to-roll printed device performance using evaporated silver electrode with a PCE of *ca* 11%.[44]

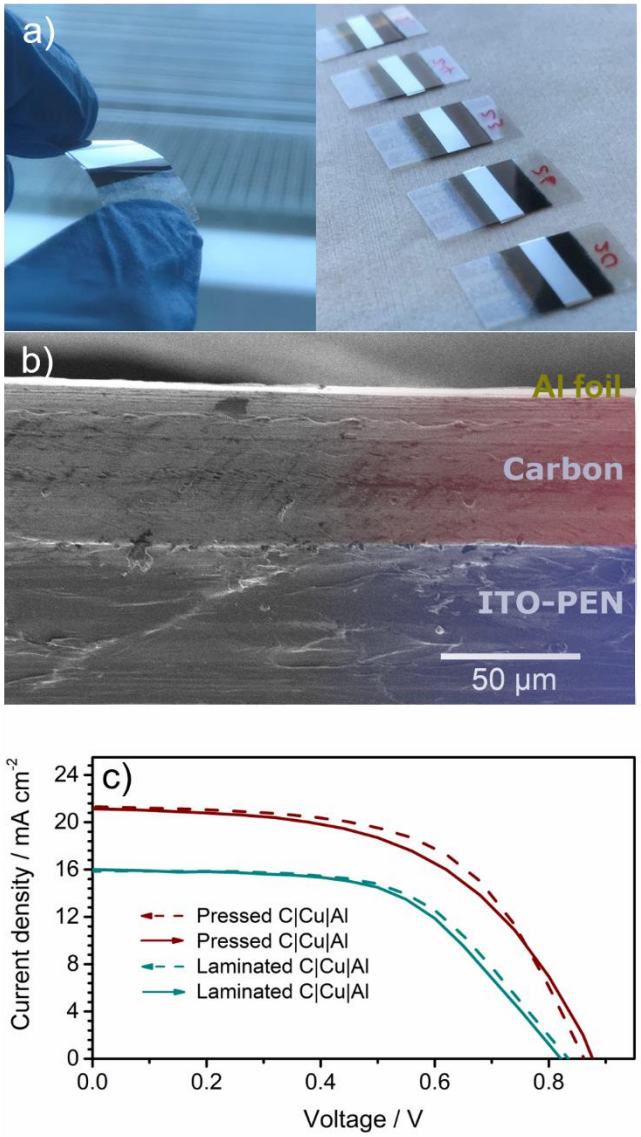

Figure 5. (a) Photographs, (d) cross-section SEM image, and (c) *J-V* curves (0.100 V s^{-1}; arrows show the scan direction; 1 sun) for the flexible roll-to-roll printed PSC devices made with aluminium-supported carbon electrodes. Photographs show laminated devices, while SEM data are for the pressed electrodes. In panel (c), *J-V* curves are shown for the devices with pressed (*dark red*) and laminated (*teal*) carbon electrodes. Overall device structure was TCO|c-SnO_2|$FA_{0.4}MA_{0.6}PbI_3$|PPDT2FBT|C|Cu|Al (see Methods for details).

To test for the possibility for direct lamination, we passed the device assembly and the carbon-aluminium electrode through a benchtop laminator without any heating applied. The PCE of the resultant devices was 8%, which is lower than with the pressed electrode (Figure 5c) and likely suggests that insufficient pressure was provided by the laminator currently available to

us – a technical parameter that can be optimised in the future. Most importantly, these results provide the first, to the best of our knowledge, demonstration of a flexible roll-to-roll-fabricated device with an electrode applied by lamination, *i.e.* a procedure that is also suitable for integration into a roll-to-roll production process.

2.4. Thermal stability assessment and recommendations for further improvements

To analyse the stability of PSCs with the laminated carbon-based electrodes described herein, we tested the capability of the glass-supported cells based on different electrodes to withstand temperature fluctuations. First, we applied an IEC 61215 photovoltaic testing protocol,[52] *viz.* 200 temperature cycles between -40 and 85 °C (**Figure S6**) over a 28 h period (**Figure 6**a). Under these conditions, PSCs with conventional evaporated Au electrodes degraded to some extent down to *ca* 84% of their initial performance. However, solar cells with carbon electrodes fabricated using the commercial carbon paste produced even worse results and were not able to sustain the performance (Figure 6a) as the electrode detached from the cell by the end of the test (**Figure S7**). At the same time, keeping the similarly-fabricated (with commercial carbon paste) devices at a constant temperature of 85 °C under N_2 in the dark for 28 h maintained their integrity and no detachment of the electrode was observed (Figure S7). These observations suggest that the temperature cycling induced mechanical damage to the solar cells, presumably due to the differences in the thermal expansion coefficients of Al, C and other components or due to the degradation of the adhesive components present in the commercial carbon paste used to fabricate the electrodes. As discussed below, we believe the latter to be the key factor.

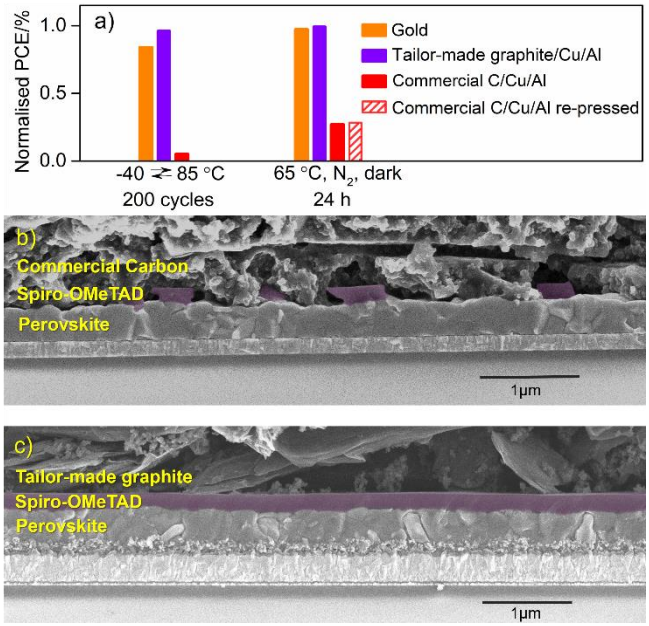

Figure 6. Thermal stability assessment of $K_{0.05}Cs_{0.25}FA_{1.30}MA_{0.23}Pb_{1.4}I_{2.7}Br_{0.46}$|spiro-OMeTAD PSCs based on evaporated Au (*orange*), C|Cu|Al prepared with a commercial paste (*red*; dashed bar shows PCE after additional pressing of the electrode after the test), and graphite|Au|Al prepared with a tailor-made graphite paste (*violet*): (a) normalised power conversion efficiency of the solar cells after 200 cycles between -40 and 85 °C under N_2 flow, and after heating at 65 °C in an N_2-filled glove-box; (b-c) cross-section SEM images of cells based on (b) C|Au|Al (commercial carbon paste) and (c) graphite|Au|Al (tailor-made graphite paste) after 24 h treatment at 65 °C in N_2-filled glove-box; purple shading highlights the spiro-OMeTAD layer.

To test if the chemical composition of the commercial carbon paste has a negative impact on the stability, we have prepared a simpler graphite paste devoid of the common adhesives/fillers in the commercial products (see Methods), and used this tailor-made precursor to produce corresponding graphite-based electrodes and PSCs following the procedures in Figure 1. Such devices performed satisfactorily during the IEC 61215 temperature cycling protocol with only a minor decline in the performance to *ca* 95% of the original value, in contrast to the more significant deterioration observed with a gold electrode of 84% (Figure 6a). Moreover, the performance of the devices based on these tailor-made graphite electrodes was again comparable to that of the PSCs with conventional evaporated Au (Table S2).

Analysing the thermal stability further, we performed constant temperature 24 h tests at 65 °C in N_2 environment and dark conditions for solar cells based on different electrodes. These particular experiments were undertaken at 65 rather than 85 °C (as in IEC 61215 tests) to avoid

the processes resulting in the changes to the spiro-OMeTAD|perovskite interface or to the spiro-OMeTAD itself that are not associated with the electrode.[47–49] Under examined conditions, significant deterioration down to 20% of the initial photovoltaic performance was observed for the cells with the commercial-paste-based carbon electrodes (Figure 6a). Re-pressing such electrodes did not improve the efficiency to any significant extent, indicating that the loss in the performance in this case is likely caused by unfavourable changes to the layers within the cell rather than a simple thermally-induced delamination. Indeed, the cross-sectional SEM analysis of the solar cells based on the commercial paste carbon electrodes demonstrated that the spiro-OMeTAD layer was destroyed in most parts of the device following the heating step (Figure 6b). In stark contrast, devices based on the tailor-made graphite electrodes retained more than 95% of the initial performance after ageing at 65 °C for 24 h, similar to the control Au-based devices (Figure 6a). The spiro-OMeTAD HTM layer in these solar cells remained undamaged (Figure 6c and **Figure S8**).

On the basis of the above observations, we hypothesise that adhesive or other compounds that remain in the commercial carbon paste even after treatment with ethanol and mild heating (step II in Figure 1) leach into and cause the deterioration of the spiro-OMeTAD layer at higher temperatures. Solar cells fabricated with such electrodes that were pre-treated at 150 °C (*cf.* 70 °C in a regular procedure) in an attempt to remove the interferants still suffered the same degradation during storage at 65 °C (**Figure S9**). Hence, we have undertaken the thermogravimetric analysis of the commercial carbon paste used to prepare the electrodes, which demonstrated a 40% mass drop within a 300-400 °C region, which might correspond to the loss of the pernicious additives that cause degradation of the HTM layer (**Figure S10**). Based on this observation and the fact that the ethanol treatment removes the components of the paste that evaporate/decompose at temperatures below 300 °C (Figure S10), we conclude that some higher boiling point components still remain in such electrodes and negatively affect the solar cell stability.

These final results allow us to draw two important conclusions: (i) the adhesives/fillers present in the commercial carbon paste are incompatible with the PSCs, (ii) carbon-based electrodes devoid of interfering compounds can be a feasible alternative to evaporated gold as a suitable electrode for perovskite solar cells in terms of both efficiency and stability. We have to acknowledge that the tailor-made graphite-based electrode needs to be improved further to improve the adhesion to the aluminium foil, which was nevertheless sufficient for meaningful characterisation of the solar cells. Interestingly, even when the Al foil is peeled off, the graphite layer remaining on the HTM surface still allowed for the efficient operation of the devices (**Figure S11**).

On the basis of the findings summarised above, we provide the following recommendations for future developments of the carbon electrodes for the perovskite solar cells:

- the electrode substrate should undergo minimal thermal deformation to maintain the integrity of the device during temperature cycling;
- a carbon precursor paste or dispersion should be based on solvents that can be easily evaporated and should be thoroughly removed prior to application of the electrode onto the device;
- addition of an adhesive is important, but this compound(s) should be inert with respect to the key device components and have a melting point significantly higher than 85 °C; a range of resins with suitable properties might already be available and need to be tested for their compatibility;
- an ideal deposition procedure through lamination or pressing would not involve heating (as the procesure described herein) to avoid potential damage to the solar cell components, but this will ultimately depend on the properties of the optimised adhesive material; a deposition process where only the electrode is pre-heated might be a compromise solution.

3. Conclusion

In this work, we present a low-cost flexible electrode based on cheap carbon allotropes such as graphite flakes and carbon black deposited onto a modified aluminium substrate, which can be directly pressed or laminated at ambient temperature onto the surfaces of different hole-transporting materials for the fabrication of perovskite solar cells. The use of the Al foil substrate modified with a thin layer of another metal (Au, Ag, Ni or Cu) ensures an efficient contact, enhances reproducibility of the results and enables compatibility with a roll-to-roll solar cell fabrication process. Pressed carbon-based electrodes fabricated in this manner enabled essentially the same perovskite solar cell performance metrics as those provided by conventional evaporated gold. Flexible printed PSCs with pressed carbon-based electrodes also achieved efficiencies similar to those reported previously for evaporated gold and silver electrodes. Additionally, successful direct lamination of the Al-supported carbon electrodes onto flexible PSCs has been demonstrated. The presented adhesive laminatable carbon electrodes can be used as a cheap, easy to fabricate and scalable alternative to evaporated gold for research purposes like high-throughput testing of large arrays of devices at ambient temperature.

The use of a tailor-made adhesive-free graphite paste instead of a commercial precursor for the fabrication of laminatable electrodes endows the resulting perovskite solar cells with improved stability, as demonstrated over 200 cycles of the IEC 61215 photovoltaic test. The mechanical integrity of the electrode substrate-graphite interface requires further improvements, which could be achieved with the development of appropriate pressing and sealing procedures, or introduction of perovskite- and HTM-benign adhesives. Both approaches are currently being pursued in our laboratories. Overall, the present study, along with previous publications, strongly suggests that laminatable carbon presents a viable alternative to conventional evaporated metals as electrodes in perovskite solar cells produced by scalable methods, in particular *via* roll-to-roll processes.

4. Methods

Materials: For the preparation of the glass-supported devices, lead(II) iodide (ultra-dry, 99.999% metal basis), lead(II) bromide (ultra-dry, 99.999% metal basis), and caesium iodide (99.999%) were purchased from Alfa Aesar. Ethanol (absolute) was purchased from UNIVAR solutions. Potassium iodide (99.5%), copper(I) thiocyanide (99%), graphite powder (<20 μm), anhydrous N,N-dimethylformamide (99.8%), anhydrous dimethylsulphoxide (99.9%), anhydrous acetonitrile (99.8%), 2-propanol (analysis grade), 2-butoxyethanol (99%), diethyl sulphide (98%), anhydrous toluene (99.8%), titanium diisopropoxide bis(acetylacetonate) solution (TAA) (75 wt.% in isopropanol), lithium bis(trifluoromethane)sulfonimide ($LiNTf_2$) (>99%), tris-2-(1*H*-pyrazol-1-yl)-4-*tert*-butylpyridine)cobalt(III) tri[bis(trifluoromethane)sulfonimide] (FK209) (98%), 4-*tert*-butylpyridine (*t*-BP) (98%) and poly[bis(4-phenyl)(2,4,6-trimethylphenyl)amine] (PTAA, M_n = 7000-10000) were purchased from Sigma-Aldrich. Titanium dioxide 30 NRD paste, formamidinium iodide (FAI) (99.99%), and methylammonium bromide (MABr) (99.99%) were purchased from Greatcell Solar Ltd. 2,2′,7,7′-Tetrakis(N,N-di-p-methoxyphenyl-amine)-9,9′-spirobifluorene (spiro-OMeTAD) was purchased from Luminescence Technology Corp. Glass substrates 2.5 cm × 2.5 cm coated with fluorine-doped tin oxide (FTO) (15 Ω sq^{-1} sheet resistance) and laser engraved to make four individual devices were purchased from Yingkou Shangneng Photoelectric material Co., Ltd. Water purified by reverse osmosis (quoted resistivity 1 MΩ cm) was used in all experimental procedures whenever water is mentioned. High-purity N_2 (99.999%, H_2O < 3 ppm, O_2 < 2 ppm) was used where nitrogen gas is mentioned.

For the preparation of flexible solar cells, lead(II) iodide (99.9985%) and tin(IV) oxide (15 wt.% in H_2O colloidal dispersion) were purchased from Alfa Aesar. MAI (99.99%), FAI (99.99%) were purchased from Dyesol. Dichlorobenzene (99%), anhydrous N,N-dimethylformamide (99.8%) and anhydrous 2-propanol (99.5%) were purchased from Sigma-Aldrich. A 25 mm wide patterned polyethylene naphthalate (PEN) roll coated with a transparent

conductive oxide (TCO) with a sheet resistance of 8 Ω sq^{-1} (OPV8) was sourced from Solutia and Meko Print. Poly[(2,5-bis(2-hexyldecyloxy)phenylene)-alt-(5,6-difluoro-4,7-di(thiophen-2-yl)benzo[c]-[1,2,5]thiadiazole)] (PPDT2FBT) was purchased from Brilliant Materials. High-purity N_2 (99.999%, H_2O < 3 ppm, O_2 < 2ppm) was used.

For the preparation of carbon electrodes, Jelcon CH-8 carbon paste was purchased from JuJo Chemicals Co. Ltd. Carbon black Printex L6 was purchased from CaryCompany. Graphite powder (< 20 μm) and 2-butoxyethanol (>99%) were purchased from Sigma-Aldrich. Silver paste (CP1 30J) was purchased from ChipQuick. Domestic grade, approximately 12 μm thick, all-purpose aluminium foil was purchased from Castaway Caterers Foil Australia and used as received.

Preparation of the perovskite and HTM precursor solutions: The perovskite precursor solution for the glass substrate-based devices was prepared by adding 1.2 mmol PbI_2 (548.0 mg), 0.21 mmol $PbBr_2$ (77.1 mg), 0.20 mmol MABr (21.8 mg), 1.1 mol FAI (190.0 mg), 60 mmol CsI (30 μL of 2.01 M CsI in DMSO), and 40 mmol KI (20 μL of 2.00 M KI in DMSO) into 800 μL of a mixed DMF : DMSO solvent solution (4 : 1 vol.), and stirring for two hours until complete dissolution of all components.

The spiro-OMeTAD solution was prepared by mixing 6.0×10^{-5} mol spiro-OMeTAD (73 mg), 2.0×10^{-4} mol *t*-BP (28.8 μl), 2.0×10^{-4} mol $LiNTf_2$ (17 μl of 520 mg mL^{-1} solution in CH_3CN) and 1.6×10^{-6} mol FK209 (8 μl of 300 mg mL^{-1} solution in CH_3CN) in 1 mL chlorobenzene.

The CuSCN solution was prepared by dissolving 2.9×10^{-4} mol (35 mg) of the salt in 1 mL of diethyl sulphide. The PTAA solution was prepared by dissolving 10 mg of the solid in 1 ml of toluene.

The perovskite solution for the flexible substrate-based devices was prepared by dissolving 0.7 mmol (322 mg) PbI_2 and 0.28 mmol (48 mg) FAI in anhydrous N,N-dimethylformamide in a nitrogen filled glove box, and stirred at 70 °C for approximately 1 h. The solution was cooled down to ambient temperature (*ca* 22 ± 2 °C) before transferring to a slot-die head. The MAI

solution for the second step of the deposition was made by stirring 5.9 mol (400 mg) of MAI in 20 mL of anhydrous 2-propanol at ambient temperature.

The HTL solution was prepared by dissolving 1.4×10^{-4} mmol (10 mg) PPDT2FBT in 1 mL of dichlorobenzene.

Solar cell fabrication: Glass-supported solar cells had a generic structure of FTO|c-TiO_2|m-TiO_2| $K_{0.05}Cs_{0.25}FA_{1.30}MA_{0.23}Pb_{1.4}I_{2.7}Br_{0.46}$|HTM|electrode, where c-$TiO_2$ is a compact titania layer and m-TiO_2 is a mesoporous titania layer.

Laser-patterned FTO coated glass substrates were cleaned by ultrasonication (Elmasonic S 300H) for 10 min in each of the following media: 2 vol.% Hellmanex detergent in H_2O, water and isopropanol. After cleaning, the FTO was covered with a compact TiO_2 layer (*ca* 15 nm) using a custom made automatic spray pyrolysis system as follows: the substrate was heated to 500 °C on a high-precision hot-plate (Gestigkeit PZ28-3TD), sprayed with *ca* 5 mL of titanium TAA precursor solution in isopropanol (1 : 19 vol.) using a SONO.TEK ultrasonic nozzle at a flow rate of 0.5 mL min^{-1} and a height of 30 cm from the substrate, kept at 500 °C for another 10 min, and then cooled down to ambient temperature naturally. Prior to the deposition of the mesoporous titania layer, the surface of the FTO|c-TiO_2 was cleaned with UV plasma (Harick, PDC-002 at high power) for 10 min. Further, 70 µl of the mixture obtained by diluting the NR-30 TiO_2 paste with ethanol (1 : 6 wt.) was spin-coated (Laurell-150 mm) at 4000 rpm for 20 s with a ramping speed of 2000 rpm s^{-1} and the substrates were sintered at 500 °C (Gestigkeit PZ28-3TD) for 30 min to produce a *ca* 150 nm thick m-TiO_2 layer. The substrates were treated with UV-plasma using the same parameters as above and immediately transferred into a N_2-filled glovebox.

Deposition of the perovskite film was performed by spin-coating 35 µL cm^{-2} of the precursor solution using a two-step program: 1000 rpm for 10 s with a ramping speed of 1000 rpm s^{-1} followed by 6000 rpm for 20 s with a ramping speed of 6000 rpm s^{-1}. Chlorobenzene (150 µL) was poured into the centre of the spinning substrate approximately 6 s prior to the end of the

second step. Immediately after spin-coating, samples were annealed at 120 °C (IKA RCT basic) for 30 min, and then allowed to cool down to the ambient temperature naturally.

Further, a layer of the required HTM was deposited following the procedures below. Spiro-OMeTAD: 35 µL of the solution was spin-coated at 3000 rpm for 30 s with a ramping speed of 3000 rpm s^{-1}; devices were then removed from the N_2-filled glove-box and aged in air in a dry box (<10% relative humidity) at ambient temperature for *ca* 12 h to oxidise spiro-OMeTAD. CuSCN: 50 µL of the solution were dropped onto a substrate that was already spinning at 5000 rpm; rotation was continued for another 30 seconds; devices were then stored in the N_2-filled glovebox until the electrode deposition. This procedure was previously reported by Arora *et al*.[51] PTAA: 25 µL of the PTAA solution was spin-coated at 1800 rpm for 30 s followed by annealing at 60 °C for 10 min.

The final step of the cell fabrication, *viz.* electrode deposition, was undertaken outside the glovebox.

Control glass-supported devices with gold electrodes were prepared using the conventional method by thermal evaporation (DDHightech GCMO3CR) through a circular shadow mask (area 0.16 cm^2) at a fixed rate of 2 Å s^{-1} at 5×10^{-6} torr with a constant rotation of the sample stage. Carbon electrode fabrication and deposition procedures are described in a separate section below.

Flexible solar cells had a generic structure of TCO|c-SnO_2|$FA_{0.4}MA_{0.6}PbI_3$|PPDT2FBT|carbon (c-SnO_2 – compact tin(IV) oxide layer) and were fabricated using the CSIRO roll-to-roll facilities[44] except for the deposition of the carbon electrode.

All the roll-to-roll experiments were carried under ambient conditions in a fume hood cabinet using a custom-made slot-die setup on a commercial roll-to-roll coater (Mini-Labo, Yasui Seki). The coating speed was controlled by a built-in controller of the roll-to-roll coater while the solution flow through the slot-die head was controlled by a syringe pump. The SnO_2 aqueous solution was coated using the microgravure method (line speed of 0.3 mL min^{-1}) followed by

annealing at 130 °C for 2 min. The TCO|SnO_2 substrate film was rewound and the first perovskite precursor solution (PbI_2 + FAI) was slot-die coated at a rolling rate of 0.3 mL min^{-1} and dispensing rate of 16-20 µL min^{-1}. A blower was installed 7 cm behind and 4 cm above the solution head and 20-25 L min^{-1} of nitrogen was blown onto the continuously moving wet film. The film was then rewound as quickly as possible and the MAI solution was applied at the rolling rate of 0.3 m min^{-1} and dispensing rate of 60 µL min^{-1} under nitrogen flow; in this case, the rate was 15 L min^{-1} while the distance was 13 cm behind and 4 cm above the solution head. PPDT2FBT solution was deposited at a rolling rate of 0.3 m min^{-1} and dispensing rate of 25 µL min^{-1} under 10 L min^{-1} nitrogen flow.

Carbon electrode preparation and fabrication: *Tailor-made carbon paste* was prepared as follows: graphite powder (5 g) and carbon black (1 g) were mixed with 5 mL of isopropanol and 1 mL of 2-butoxyethanol, and ball milled (Fritsch Pulverisette 6) for 30 min. *Commercial* Jelcon CH-8 carbon paste was used as received.

To prepare the electrode, an aluminium foil substrate was cleaned by wiping with ethanol and either used for carbon deposition directly, or pre-coated with a *ca* 100 nm thin layer of metal (gold, nickel or copper) by evaporation, or with a *ca* 25 µm layer of a silver paste. Gold was deposited using a thermal evaporator (DDHightech GCMO3CR) at a fixed rate of 2 Å s^{-1} at 5 × 10^{-6} torr with a constant rotation of a stage. Ni and Cu were deposited using a AC/DC sputtering unit (Anatech Hummer BC-20) at a DC power of 200 and 150 watts, respectively, under an argon gas flow of 10 sccm. Commercial silver paste (2 g) was diluted to make a slurry by adding *ca* 0.5 ml of 2-butoxyethanol and deposited by manual doctor blading under ambient conditions using a glass slide and a layer of a *ca* 30 µm thick Kapton tape to define the thickness, although the resulting thickness was typically *ca* 25 µm. The thickness of the carbon layers was measured using a Dektak 150 profilometer, while the conductivity was quantified using a Jandell RM3000 four-point probe.

A carbon layer was deposited on top of the aluminium substrate or metal-coated aluminium substrate by automated doctor blading (MTVmesstechnik CX202) of approximately 5 mg cm^{-2} of the Jelcon CH-8 paste at a rate of 9 mm s^{-1} and the height adjusted to 80 μm. A tailor-made paste was coated using a glass slide using two layers of a *ca* 30 μm thick Kapton tape to define the thickness. After deposition, the Al-supported-commercial carbon films were immersed in ethanol for 30 min, which was continuously stirred using a Teflon-lined magnetic bar. Further, the electrodes were dried in air (Contherm thermotic 2000 oven) at 65 °C for two hours, cooled to the ambient temperature and cut into 1.2 cm × 0.7 cm pieces. Finally, four of these electrodes were applied onto four devices simultaneously using a conventional hydraulic press (Metalmaster PP-10HD) at 20 MPa for 2 min; to avoid breaking the glass substrate, the cell and electrode were sandwiched between *ca* 1.5 mm thick rubber (Translucent silicon rubber RS Component Pty Ltd). The Supplementary Video shows the key stages of the electrode preparation and application procedures.

To fabricate flexible devices, the carbon electrode was deposited either by pressing or lamination. In the former case, the carbon electrode was cut into 3 cm × 0.35 cm pieces and pressed on top of the TCO|c-SnO_2|$FA_{0.4}MA_{0.6}PbI_3$|PPDT2FBT assemblies following the same procedures as those used for the glass-supported devices. Lamination was achieved by passing the TCO|c-SnO_2|$FA_{0.4}MA_{0.6}PbI_3$|PPDT2FBT assemblies with carbon-aluminium electrodes through the laminator (Peach 3500 photo pouch laminator) at ambient temperature, *i.e.* no heating was applied during the lamination process.

Photovoltaic characterisation: Testing of the glass-supported solar cells was undertaken using a high throughput characterisation system developed by Surmiak *et al.*[53] To ensure robust contact between pins and the cell electrodes, small areas of solder were applied on the sides of the devices. The devices were illuminated by a Abet Technologies Sun 3000 class AAA solar simulator calibrated at AM 1.5 (100 $mWcm^{-2}$) intensity through a mask with an aperture size of 0.16 cm^2 and *J-V* data were collected using a 16-channel Bio-Logic VMP3 electrochemical

workstation. The current density (*J*) – voltage (*V*) scans were recorded in both reverse (1.2 V → -0.1 V) and forward (-0.1 V → 1.2 V) directions with 0.010 V steps and settling times of 100 ms (nominal scan rate 0.100 V s^{-1}). Prior to the measurement, devices were illuminated for 10 s for stabilisation. The steady-state efficiency was measured by recording the photocurrent at a fixed potential that corresponded to the maximum power point in the reverse *J-V* scan.

The *J-V* characteristics of the flexible devices were measured in an inert atmosphere with a computer-controlled Keithley 2400 Source Measure Unit. A 150 W Xenon lamp (Newport) coupled with an AM 1.5G solar spectrum filter was used as the light source. Device area was defined by an overlap of the strip of printed ITO (3.5 mm wide) on the flexible substrate and strip of carbon electrode (4 mm wide) with no mask applied to achieve a 0.14 cm^2 cell area. Prior to each measurement, devices were exposed to the light source for approximately 10 s. Characterisation was undertaken by recording reverse scans (from open-circuit to short-circuit) and forward scan (from short-circuit to open-circuit) at 0.020 V steps and 100 ms dwell time (nominal scan rate 0.200 V s^{-1}).

Electrochemical impedance spectroscopic (EIS) data were collected using a Zahner Zennium electrochemical workstation equipped with a frequency response analyser module. Measurements were undertaken using a sinusoidal potential perturbation with an amplitude of 0.010 V within a frequency range from 2 MHz to 0.1 Hz. During measurements, solar cells were illuminated with a white LED light, the output intensity of which was adjusted to provide the same photocurrent as that measured under 1 sun irradiation using the Abet Technologies Sun 3000 class AAA source. Modelling of the EIS data was based on an equivalent circuit described in the main text using the Z-View software (Scribner Associates).

Solar cell durability tests: Shelf stability of the devices was studied by storing PSCs in a dry cabinet where the relative humidity varied within a 2-20% range. Periodic characterisation of the solar cells resulted in their exposure to ambient conditions for approximately 1 h. For all devices, forward and backward *J-V* scans were recorded followed by a steady-state efficiency

measurement. Data derived from the steady-state measurements were used for reporting the evolution of the performance during storage.

For the thermocycling test, a Linkam system (TP94 + LNP + custom-built Linkam stage) was used. The stage was continuously purged with N_2. Using a purpose-built software control system (Labview), the temperature of the solar cell (detected by PT100 thermocouple attached to the solar cell) was cycled between -40 °C and 85 °C at a rate of 1.5 deg s^{-1} and maintained at the maximal and minimal temperature, *i.e.* -40 °C and 85 °C, for 2 min at each cycle.

Scanning electron microscopy: Scanning electron microscopic (SEM) images were collected on a FEI Magellan 400 XHR FEGSEM microscope at a voltage of 3 kV and probe current 6.3 pA. For side-view imaging, complete glass-supported devices without a silver paste interlayer were cracked using a glass cutter and pliers. This approach was not effective when applied to the PSC containing a Ag-paste, which was cracked using a hydraulic press under excessively high pressure (40 Mpa). Flexible devices were cut for analysis using a paper cutter. The samples were immobilised in a TED PELLA, Inc. cross-sectional side-view holder and pre-coated with a *ca* 1 nm layer of iridium to minimise charging effects.

Supporting Information
Supporting Information is available from the Wiley Online Library or from the author.

Acknowledgements
This work was funded by the Australian Centre for Advanced Photovoltaics and Australian Renewable Energy Agency. ANS also acknowledges the financial support from ARC (Centre of Excellence CE140100012; Future Fellowship FT200100317). Monash Centre for Electron Microscopy (MCEM) and Melbourne Centre for Nano fabrication (MCN) are acknowledged for providing access to their facilities. The authors are grateful to Dr T. Zhang, A. Surmiak, Dr. N. Peris, Dr. D. Senevirathna and Dr. N. Pai from Monash University for the experimental support throughout this study.

References

[1] A. Abate, J. P. Correa-Baena, M. Saliba, M. S. Su'ait, F. Bella, *Chem. - A Eur. J.* **2018**, *24*, 3083.
[2] Z. Song, C. L. McElvany, A. B. Phillips, I. Celik, P. W. Krantz, S. C. Watthage, G. K. Liyanage, D. Apul, M. J. Heben, *Energy Environ. Sci.* **2017**, *10*, 1297.
[3] Z. Li, Y. Zhao, X. Wang, Y. Sun, Z. Zhao, Y. Li, H. Zhou, Q. Chen, *Joule* **2018**, *2*, 1559.

[4] W. S. Yang, J. H. Noh, N. J. Jeon, Y. C. Kim, S. Ryu, J. Seo, S. Il Seok, *Science* **2015**, *348*, 1234.
[5] D. Bi, C. Yi, J. Luo, J. D. Décoppet, F. Zhang, S. M. Zakeeruddin, X. Li, A. Hagfeldt, M. Grätzel, *Nat. Energy* **2016**, *1*, 1.
[6] E. H. Jung, N. J. Jeon, E. Y. Park, C. S. Moon, T. J. Shin, T. Y. Yang, J. H. Noh, J. Seo, *Nature* **2019**, *567*, 511.
[7] M. Jeong, I. W. Choi, E. M. Go, Y. Cho, M. Kim, B. Lee, S. Jeong, Y. Jo, H. W. Choi, J. Lee, J. H. Bae, S. K. Kwak, D. S. Kim, C. Yang, *Science* **2020**, *369*, 1615.
[8] J. Jeong, M. Kim, J. Seo, H. Lu, P. Ahlawat, A. Mishra, Y. Yang, M. A. Hope, F. T. Eickemeyer, M. Kim, Y. J. Yoon, I. W. Choi, B. P. Darwich, S. J. Choi, Y. Jo, J. H. Lee, B. Walker, S. M. Zakeeruddin, L. Emsley, U. Rothlisberger, A. Hagfeldt, D. S. Kim, M. Grätzel, J. Y. Kim, *Nature* **2021**, *592*, 381.
[9] http://goldprice.com.au/, accessed: July, **2021**.
[10] *International Technology Roadmap for Photovoltaic*, https://itrpv.vdma.org/en/, accessed: July, **2021**.
[11] N. L. Chang, A. W. Yi Ho-Baillie, P. A. Basore, T. L. Young, R. Evans, R. J. Egan, *Prog. Photovoltaics Res. Appl.* **2017**, *25*, 390.
[12] K. Domanski, J. P. Correa-Baena, N. Mine, M. K. Nazeeruddin, A. Abate, M. Saliba, W. Tress, A. Hagfeldt, M. Grätzel, *ACS Nano* **2016**, *10*, 6306.
[13] Y. Kato, L. K. Ono, M. V. Lee, S. Wang, S. R. Raga, Y. Qi, *Adv. Mater. Interfaces* **2015**, *2*, 1500195.
[14] M. S. Seetharaman, P. Nagarjuna, P. N. Kumar, S. P. Singh, M. Deepa, M. A. G. Namboothiry, *Phys. Chem. Chem. Phys.* **2014**, *16*, 24691.
[15] T. Leijtens, G. E. Eperon, S. Pathak, A. Abate, M. M. Lee, H. J. Snaith, *Nat. Commun.* **2013**, *4*, 1.
[16] J. Zhao, X. Zheng, Y. Deng, T. Li, Y. Shao, A. Gruverman, J. Shield, J. Huang, *Energy Environ. Sci.* **2016**, *9*, 3650.
[17] U. Yogeswaran, S. Chen, *Anal. Lett.* **2008**, *41*, 210.
[18] I. Švancara, K. Vytřas, K. Kalcher, A. Walcarius, J. Wang, *Electroanalysis* **2009**, *21*, 7.
[19] P. Avouris, Z. Chen, V. Perebeinos, *Nat. Nanotechnol.* **2007**, *2*, 605.
[20] M. Wu, M. Sun, H. Zhou, J. Y. Ma, T. Ma, *Adv. Funct. Mater.* **2020**, *30*, 1906451.
[21] L. Fagiolari, F. Bella, *Energy Environ. Sci.* **2019**, *12*, 3437.
[22] M. Hadadian, J. H. Smått, J. P. Correa-Baena, *Energy Environ. Sci.* **2020**, *13*, 1377.
[23] A. Mei, X. Li, L. Liu, Z. Ku, T. Liu, Y. Rong, M. Xu, M. Hu, J. Chen, Y. Yang, M. Grätzel, H. Han, *Science* **2014**, *345*, 295.
[24] A. K. Jena, A. Kulkarni, T. Miyasaka, *Chem. Rev.* **2019**, *119*, 3036.
[25] A. Kharitonov, J. Zha, M. Dubois, *J. Fluor. Chem.* **2015**, *178*, 279.
[26] W. Dai, S. J. Kim, W. K. Seong, S. H. Kim, K. R. Lee, H. Y. Kim, M. W. Moon, *Sci. Rep.* **2013**, *3*, 1.
[27] Z. Yu, B. Chen, P. Liu, C. Wang, C. Bu, N. Cheng, S. Bai, Y. Yan, X. Zhao, *Adv. Funct. Mater.* **2016**, *26*, 4866.
[28] J.-M. Yun, J.-S. Yeo, J. Kim, H.-G. Jeong, D.-Y. Kim, Y.-J. Noh, S.-S. Kim, B.-C. Ku, S.-I. Na, *Adv. Mater.* **2011**, *23*, 4923.
[29] Q. Luo, Y. Zhang, C. Liu, J. Li, N. Wang, H. Lin, *J. Mater. Chem. A* **2015**, *3*, 15996.
[30] Q. Luo, H. Ma, Q. Hou, Y. Li, J. Ren, X. Dai, Z. Yao, Y. Zhou, L. Xiang, H. Du, H. He, N. Wang, K. Jiang, H. Lin, H. Zhang, Z. Guo, *Adv. Funct. Mater.* **2018**, *28*, 1706777
[31] T. Dürkop, S. A. Getty, E. Cobas, M. S. Fuhrer, *Nano Lett.* **2003**, *4*, 35.
[32] I. Jeon, A. Shawky, S. Seo, Y. Qian, A. Anisimov, E. I. Kauppinen, Y. Matsuo, S. Maruyama, *J. Mater. Chem. A* **2020**, *8*, 11141.
[33] *Single walled carbon nanotubes, Product no755710, Sigma-Aldrich,*

https://www.sigmaaldrich.com/catalog/product/aldrich/755710, accessed: July, **2021**.
[34] *Multiwalled carbon nanotube, Product no 755133, Sigma-Aldrich*, https://www.sigmaaldrich.com/catalog/product/aldrich/755133, accessed: July, **2021**.
[35] Z. Wu, Z. Liu, Z. Hu, Z. Hawash, L. Qiu, Y. Jiang, L. K. Ono, Y. Qi, *Adv. Mater.* **2019**, *31*, 1804284.
[36] G. A. Sepalage, S. Meyer, A. Pascoe, A. D. Scully, F. Huang, U. Bach, Y. B. Cheng, L. Spiccia, *Adv. Funct. Mater.* **2015**, *25*, 5650.
[37] C. Tian, A. Mei, S. Zhang, H. Tian, S. Liu, F. Qin, Y. Xiong, Y. Rong, Y. Hu, Y. Zhou, S. Xie, H. Han, *Nano Energy* **2018**, *53*, 160.
[38] H. Wei, J. Xiao, Y. Yang, S. Lv, J. Shi, X. Xu, J. Dong, Y. Luo, D. Li, Q. Meng, *Carbon* **2015**, *93*, 861.
[39] H. Zhang, J. Xiao, J. Shi, H. Su, Y. Luo, D. Li, H. Wu, Y. B. Cheng, Q. Meng, *Adv. Funct. Mater.* **2018**, *28*, 1802985.
[40] H. Su, J. Xiao, Q. Li, C. Peng, X. Zhang, C. Mao, Q. Yao, Y. Lu, Z. Ku, J. Zhong, W. Li, Y. Peng, F. Huang, Y. B. Cheng, *Mater. Sci. Semicond. Process.* **2020**, *107*, 104809.
[41] Z. Li, S. A. Kulkarni, P. P. Boix, E. Shi, A. Cao, K. Fu, S. K. Batabyal, J. Zhang, Q. Xiong, L. H. Wong, N. Mathews, S. G. Mhaisalkar, *ACS Nano* **2014**, *8*, 6797.
[42] J. W. Lee, I. Jeon, H. S. Lin, S. Seo, T. H. Han, A. Anisimov, E. I. Kauppinen, Y. Matsuo, S. Maruyama, Y. Yang, *Nano Lett.* **2019**, *19*, 2223.
[43] Y. Yang, M. T. Hoang, D. Yao, N. D. Pham, V. T. Tiong, X. Wang, W. Sun, H. Wang, *Sol. Energy Mater. Sol. Cells* **2020**, *210*, 110517.
[44] Y. J. Heo, J. E. Kim, H. Weerasinghe, D. Angmo, T. Qin, K. Sears, K. Hwang, Y. S. Jung, J. Subbiah, D. J. Jones, M. Gao, D. Y. Kim, D. Vak, *Nano Energy* **2017**, *41*, 443.
[45] J. Bisquert, L. Bertoluzzi, I. Mora-Sero, G. Garcia-Belmonte, *J. Phys. Chem. C* **2014**, *118*, 18983.
[46] S. M. Yoo, S. J. Yoon, J. A. Anta, H. J. Lee, P. P. Boix, I. Mora-Seró, *Joule* **2019**, *3*, 2535.
[47] A. K. Jena, Y. Numata, M. Ikegami, T. Miyasaka, *J. Mater. Chem. A* **2018**, *6*, 2219.
[48] G. Tumen-Ulzii, C. Qin, T. Matsushima, M. R. Leyden, U. Balijipalli, D. Klotz, C. Adachi, *Sol. RRL* **2020**, *4*, 2000305.
[49] X. Zhao, H. S. Kim, J. Y. Seo, N. G. Park, *ACS Appl. Mater. Interfaces* **2017**, *9*, 7148.
[50] L. Calió, S. Kazim, M. Grätzel, S. Ahmad, *Angew. Chemie Int. Ed.* **2016**, *55*, 14522.
[51] N. Arora, M. I. Dar, A. Hinderhofer, N. Pellet, F. Schreiber, S. M. Zakeeruddin, M. Grätzel, *Science* **2017**, *358*, 768.
[52] P. Holzhey, M. Saliba, *J. Mater. Chem. A* **2018**, *6*, 21794.
[53] M. A. Surmiak, T. Zhang, J. Lu, K. J. Rietwyk, S. R. Raga, D. P. McMeekin, U. Bach, *Sol. RRL* **2020**, *4*, 2000097.